

The Absolute Magnitudes of 1991T-like Supernovae*

M. M. PHILLIPS,¹ C. ASHALL,² CHRISTOPHER R. BURNS,³ CARLOS CONTRERAS,¹
L. GALBANY,^{4,5} P. HOEFLICH,⁶ E. Y. HSIAO,⁶ NIDIA MORRELL,¹
PETER NUGENT,^{7,8} SYED A. UDDIN,⁹ E. BARON,¹⁰ WENDY L. FREEDMAN,¹¹
CHELSEA E. HARRIS,¹² KEVIN KRISCIUNAS,⁹ S. KUMAR,⁶ J. LU,⁶ S. E. PERSSON,³
ANTHONY L. PIRO,³ ABIGAIL POLIN,^{3,13} SHAHBANDEH, M.,⁶
MAXIMILIAN STRITZINGER,¹⁴ AND NICHOLAS B. SUNTZEFF⁹

¹*Carnegie Observatories, Las Campanas Observatory, Casilla 601, La Serena, Chile*

²*Department of Physics, Virginia Polytechnic Institute and State University, 850 West Campus Drive, Blacksburg, VA 24061, USA*

³*Observatories of the Carnegie Institution for Science, 813 Santa Barbara St., Pasadena, CA 91101, USA*

⁴*Institute of Space Sciences (ICE, CSIC), Campus UAB, Carrer de Can Magrans, s/n, E-08193 Barcelona, Spain.*

⁵*Institut d'Estudis Espacials de Catalunya (IEEC), E-08034 Barcelona, Spain.*

⁶*Department of Physics, Florida State University, 77 Chieftan Way, Tallahassee, FL 32306, USA*

⁷*Department of Astronomy, University of California, Berkeley, USA*

⁸*Lawrence Berkeley National Laboratory, USA*

⁹*George P. and Cynthia Woods Mitchell Institute for Fundamental Physics and Astronomy, Texas A&M University, Department of Physics and Astronomy, College Station, TX 77843, USA*

¹⁰*University of Oklahoma 440 W. Brooks, Rm 100, Norman, Oklahoma, 73019, USA*

¹¹*Department of Astronomy and Astrophysics, University of Chicago, 5640 S. Ellis Ave, Chicago, IL 60637, USA*

¹²*Center for Data Intensive and Time Domain Astronomy, Department of Physics and Astronomy, Michigan State University, East Lansing, MI 48824, USA*

¹³*TAPIR, Walter Burke Institute for Theoretical Physics, Caltech, 1200 East California Boulevard, Pasadena, CA 91125, USA*

¹⁴*Department of Physics and Astronomy, Aarhus University, Ny Munkegade 120, DK-8000 Aarhus C, Denmark*

Submitted to ApJ

ABSTRACT

1991T-like supernovae are the luminous, slow-declining extreme of the Branch shallow-silicon (SS) subclass of Type Ia supernovae. They are distinguished by extremely weak Ca II H & K and Si II λ 6355 and strong Fe III absorption features in their optical spectra at pre-maximum phases, and have long been suspected to be over-luminous compared to normal Type Ia supernovae. In this paper, the pseudo equivalent width of the Si II λ 6355 absorption obtained at light curve phases from $\leq +10$ days is combined with the morphology of the *i*-band light curve to identify a sample of 1991T-like supernovae in the Carnegie Supernova Project II. Hubble

* This paper includes data gathered with the 6.5 meter Magellan telescopes at Las Campanas Observatory, Chile.

diagram residuals show that, at optical as well as near-infrared wavelengths, these events are over-luminous by $\sim 0.1\text{--}0.5$ mag with respect to the less extreme Branch SS (1999aa-like) and Branch core-normal supernovae with similar B -band light curve decline rates.

Keywords: Type Ia supernovae (1728), Supernovae (1668), Observational cosmology (1146)

1. INTRODUCTION

Type Ia supernovae (SNe Ia) provide a powerful tool for modern cosmology. Although they are not perfect standard candles, the luminosities and colors of SNe Ia vary smoothly with light curve width (Phillips 1993; Hamuy et al. 1996; Riess et al. 1996; Phillips et al. 1999; Burns et al. 2014, 2018) making it possible to determine reliable distances to a precision of 5–10%, especially when near-infrared (NIR) photometry is available (e.g., Krisciunas et al. 2004; Phillips 2012; Burns et al. 2018; Avelino et al. 2019). Observations of SNe Ia have provided the most precise local measurements of the Hubble constant to date (e.g., Riess et al. 2016; Dhawan et al. 2018; Burns et al. 2018; Freedman et al. 2019; Riess et al. 2021; Uddin et al. 2022) and led to the discovery of the accelerated expansion of the Universe (Riess et al. 1998; Perlmutter et al. 1999).

At the luminous extreme of the absolute magnitude versus light-curve width relation for SNe Ia are the slow-declining 1991T-like (henceforth “91T-like”) events, named after the well-observed SN 1991T (Filippenko et al. 1992; Phillips et al. 1992; Ruiz-Lapuente et al. 1992; Jeffery et al. 1992; Mazzali et al. 1995; Gómez et al. 1996; Lira et al. 1998; Blondin et al. 2012; Silverman et al. 2012a). At pre-maximum phases, this supernova (SN) displayed strong absorption features of Fe III at optical wavelengths, whereas the Si II, Ca II, and S II features that typify normal SNe Ia¹ spectra at these epochs were extremely weak or missing altogether. By two weeks after maximum light, however, the spectrum of SN 1991T was essentially that of a normal Type Ia event. The decline rate of the B -band light curve was measured to be $\Delta m_{15}(B) = 0.95 \pm 0.05$ mag² (Lira et al. 1998), and the absolute magnitude, $M(B)$, at maximum may have been as much as 0.5 mag brighter than those of normal SNe Ia with similar decline rates (Mazzali et al. 1995; Saha et al. 2001). Like other slow-declining SNe Ia, the 91T-like SNe are associated with star-forming galaxies (e.g., see Hamuy et al. 2000).

A few years after the discovery of SN 1991T, Nugent et al. (1995) demonstrated that the luminosity versus decline rate relationship for SNe Ia was accompanied by

¹ In this paper, a “normal SN Ia” refers to the “core-normal” definition of Branch et al. (2006).

² $\Delta m_{15}(B)$ is defined as the amount in magnitudes that the SN fades in the first 15 days following the epoch of B -band maximum (Phillips 1993).

a parallel sequence of smoothly varying spectral features at maximum light. These spectral variations were ascribed to differences in temperature corresponding to the amount of ^{56}Ni produced in the explosion, with 91T-like events representing the highest temperatures (largest ^{56}Ni masses). The discovery of SN 1999aa (Filippenko et al. 1999), which showed a pre-maximum spectral evolution intermediate between that of SN 1991T and normal SNe Ia (Li et al. 2001b; Garavini et al. 2004), lent credence to the idea that 91T-like events are simply extreme examples of normal SNe Ia (Branch 2001; Garavini et al. 2004).

Figure 1 displays spectra at three different phases of SN 1991T, SN 1999aa, and the normal SNe 1999ee and 2011fe (Hamuy et al. 2002b; Stritzinger et al. 2002). At pre-maximum epochs, the spectrum of SN 1991T is remarkable for the extreme weakness of the Ca II H & K and Si II $\lambda 6355$ absorption features, which are clearly visible in the spectra of SN 1999ee and SN 2011fe, although in the case of the day -9 spectrum of SN 1999ee, the Ca II and Si II absorptions are dominated by a high-velocity component (Mazzali et al. 2005). At these pre-maximum phases, the Ca II and Si II absorptions in the pre-maxima spectra of SN 1999aa are seen to be intermediate in strength between SN 1991T and SN 1999ee. At two weeks past maximum, however, the spectra of all four SNe show only minor differences. Note that the $\Delta m_{15}(B)$ values reported in the literature for SN 1999aa (0.85 ± 0.08 ; Jha et al. 2006) and SN 1999ee (0.94 ± 0.06 ; Stritzinger et al. 2002) are similar to within the errors to that of SN 1991T, while SN 2011fe had a slightly faster decline rate of 1.10 ± 0.04 (Pereira et al. 2013).

Because they are among the most luminous SNe Ia, 91T-like events will inevitably be included in distant samples used to study cosmology. A better understanding of these objects is therefore crucial not only to deciphering the progenitors and explosion mechanism, but also to avoid possible systematic errors in cosmological samples of SNe Ia. In this paper, we examine the absolute magnitudes of a sample of 91T-like SNe observed during the course of the second phase of the Carnegie Supernova Project (CSP-II; Phillips et al. 2019). In §2, a new method for classifying them based on photometry and one or more optical spectra taken between -10 and $+10$ days with respect to the epoch of B maximum is presented. In §3, this technique is employed to identify ten 91T-like SNe observed by CSP-II. A brief description of the optical spectral evolution of 91T-like SNe is also included in this section. Next, in §4, the optical and near-infrared (NIR) Hubble diagram residuals of the 91T-like events in the CSP-II sample are compared to 1999aa-like (henceforth “99aa-like”) and normal SNe Ia with similar decline rates. Finally, in §5, our conclusions are summarized.

2. IDENTIFYING 91T-LIKE SUPERNOVAE

Branch et al. (2006) devised a system for classifying SNe Ia into four subtypes based on the pseudo-equivalent widths (pEW) of the Si II $\lambda\lambda 5972, 6355$ absorption features near maximum light. Figure 2a shows this “Branch diagram” for SNe Ia observed spectroscopically by the CfA Supernova Group (Blondin et al. 2012) and the first

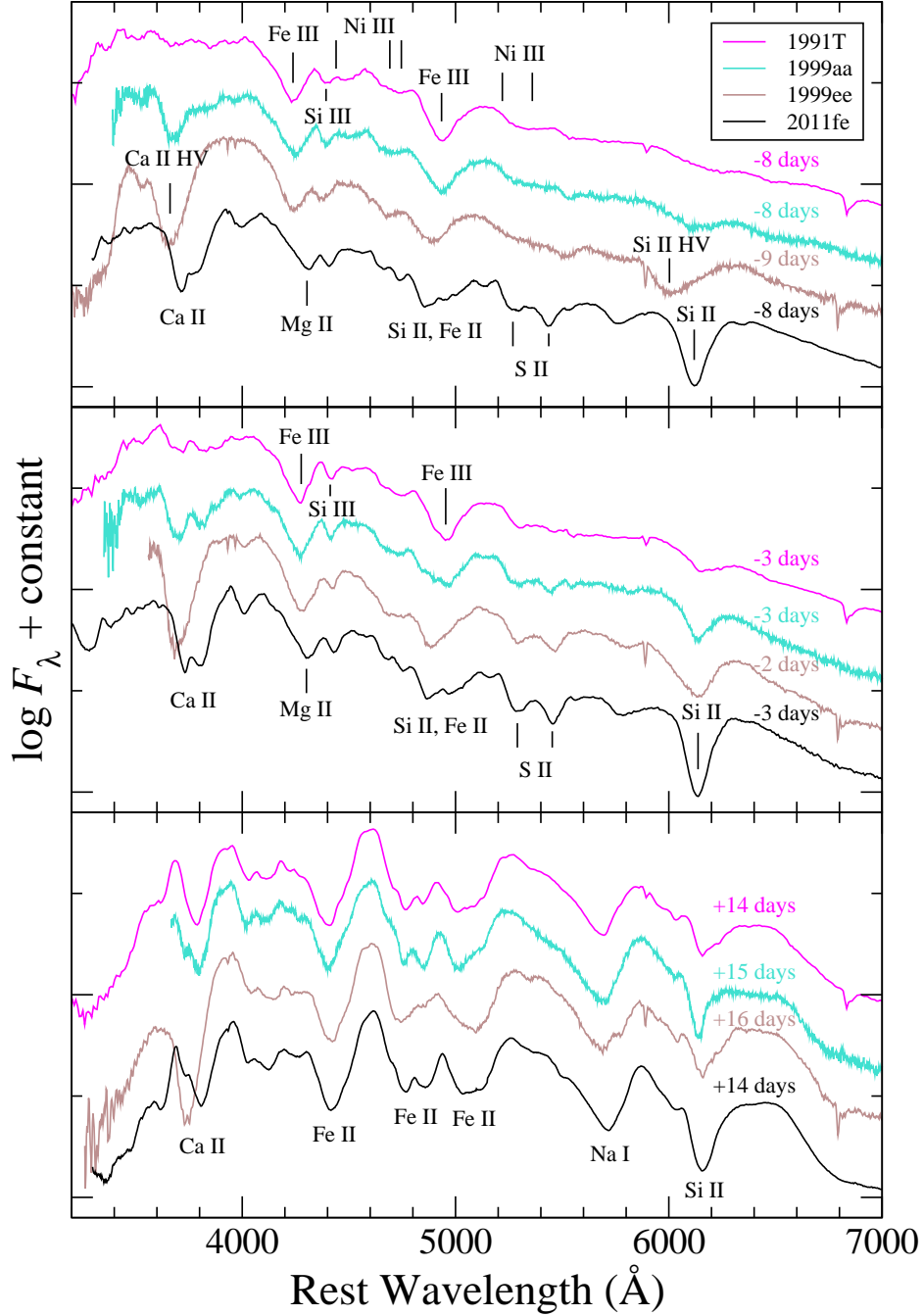


Figure 1. Optical spectra of SN 1991T obtained at -8 days, -3 days, and $+14$ days with respect to the time of maximum light in the B -band. Spectra of SN 1999aa, SN 1999ee, and SN 2011fe at similar phases are plotted for comparison. The spectra for SN 1991T are taken from Phillips et al. (1992), those of SN 1999aa from Blondin et al. (2012), those of SN 1999ee from Hamuy et al. (2002b), and those of SN 2011fe from Pereira et al. (2013). Each spectrum was corrected for Galactic reddening using the the Schlafly & Finkbeiner (2011) recalibration of the Schlegel, Finkbeiner & Davis (1998) infrared dust maps. In addition, based on SNooPy (Burns et al. 2011) fits to the photometry using the color versus decline rate calibration of Burns et al. (2014), corrections for host galaxy reddenings of $E(B - V)_{\text{host}} = 0.15$ and 0.31 mag were applied to the spectra of SN 1991T and SN 1999ee, respectively, while $E(B - V)_{\text{host}}$ was assumed to be zero for both SN 1999aa and SN 2011fe.

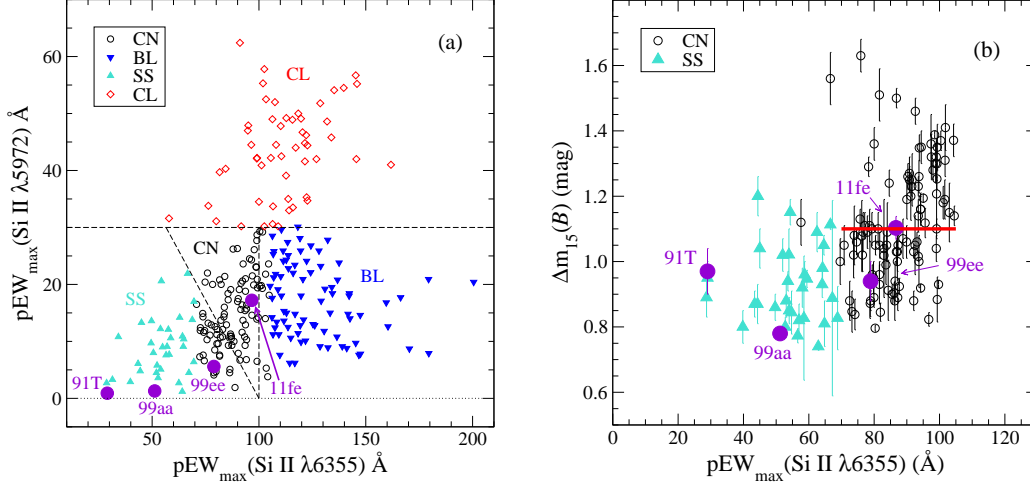


Figure 2. (a) Branch diagram for SNe Ia observed by the CfA Supernova Group and the CSP-I. The dashed lines approximate the boundaries between the different subtypes adopted by Branch et al. (2009) (See Figure 10 of Silverman et al. 2012b)), while the different colors correspond to the boundaries assumed by Folatelli et al. (2013), which are similar to those used by Blondin et al. (2012); (b) The light curve decline rate parameter, $\Delta m_{15}(B)$, plotted versus the pseudo-equivalent width of the Si II $\lambda 6355$ absorption for the Branch SS (green triangles) and CN (black circles) subtypes in the CfA Supernova Group and the CSP-I samples. In this paper, we refer to CN events lying below the red horizontal line ($\Delta m_{15}(B) < 1.1$) as the “slow-declining Branch CN” SNe (see §4).

phase of the Carnegie Supernova Project (CSP-I; Folatelli et al. 2013). Branch et al. (2009) divided the diagram into four areas delineated approximately by the dashed lines drawn in Figure 2a: CN for “core normal”, SS for “shallow silicon”, BL for “broad line”, and CL for “cool”. Blondin et al. (2012) and Folatelli et al. (2013) divided up the four areas in a slightly different manner; in this paper, we adopt the boundaries of Folatelli et al. which are indicated by the colors of the symbols in Figure 2a. A recent cluster analysis of the Branch diagram by Burrow et al. (2020) using Gaussian mixture models concluded that the general division into the CN, SS, BL, and CL groups was robust and that, when Si II velocity information is included in the analysis, the BL group appears to be distinct with respect to the other three groups.

The positions of SN 1991T and SN 1999aa are shown in Figure 2a. Both fall clearly in the SS portion of the Branch diagram, with SN 1991T having one of the smallest values of $pEW(\text{Si II } \lambda 6355)$ of any of the SNe plotted. The positions of the CN SNe 1999ee and 2011fe in the diagram are also shown for reference.

In Figure 2b, the decline rate parameter, $\Delta m_{15}(B)$, is plotted versus $pEW(\text{Si II } \lambda 6355)$ for the SS and CN SNe in the CfA and CSP I samples. The measurements for the CfA sample are taken from Blondin et al. (2012), while those for the CSP-I are from Folatelli et al. (2013). Points corresponding to SN 1991T, SN 1999aa, SN 1999ee, and SN 2011fe are indicated. Not surprisingly, this diagram resembles the region of the Branch diagram occupied by the SS and CN SNe since $pEW(\text{Si II } \lambda 5972)$ is known to correlate strongly with $\Delta m_{15}(B)$ (Hachinger et al.

2008; Folatelli et al. 2013). This plot clearly demonstrates that 91T-like SNe, and SS events in general, cannot be distinguished from many CN events on the basis of their decline rates alone.

The Branch diagram is an excellent tool for identifying 91T-like SNe, but it requires that an optical spectrum be obtained within a few days of maximum light. Often this is not the case, and so we have developed an alternative method based on the evolution of $pEW(\text{Si II } \lambda 6355)$. Figure 3a shows our measurements of $pEW(\text{Si II } \lambda 6355)$ plotted as a function of phase with respect to the epoch of B maximum, $t - t(B_{max})$, for the CN and SS SNe in the CfA and CSP-I spectroscopic samples. Again, the measurements for SN 1991T, SN 1999aa, SN 1999ee, and SN 2011fe are highlighted for reference. For the SS SNe, $pEW(\text{Si II } \lambda 6355)$ is observed to increase approximately monotonically between $-15 \text{ d} \lesssim t - t(B_{max}) \lesssim +3 \text{ d}$, and then stays roughly constant to $+10 \text{ d}$. The trajectory of SN 1991T lies at the extreme lower edge of the distribution of SS events, while that of SN 1999aa sits more or less in the middle of the SS SNe. The evolution of $pEW(\text{Si II } \lambda 6355)$ for the CN objects contrasts with that of the SS subtype in that events caught early enough display a rapid initial decline in equivalent width until $t - t(B_{max}) \sim -8 \text{ d}$, followed by a period of slowly increasing values that extends to $t - t(B_{max}) \sim +3 \text{ d}$, and then a final slow decline to $t - t(B_{max}) = +10 \text{ d}$. Inspection of the CN spectra obtained during the initial sharp decline in $pEW(\text{Si II } \lambda 6355)$ indicates that this phenomenon is due to the presence of high-velocity Si II absorption at the earliest epochs, which rapidly decays in strength. Note that this behavior is not observed for the SS SNe, implying either an absence of high-velocity Si and Ca or higher ionization conditions in the outermost ejecta.

In principle, the pseudo equivalent width of the Ca II H & K absorption feature can also be used to identify 91T-like SNe. This is illustrated in Figure 3b where $pEW(\text{Ca II H \& K})$ is plotted versus $pEW(\text{Si II } \lambda 6355)$ for light curve epochs spanning the range from $-10 \text{ d} \leq t - t(B_{max}) \leq +10 \text{ d}$ for SN 1991T, SN 1999aa, SN 1999ee, and SN 2011fe. The phases of selected spectra are labelled to indicate how the pseudo equivalent width measurements evolve as a function of time. The trajectories of the points for SN 1991T and SN 1999aa are seen to be similar but offset, with SN 1991T always displaying weaker Si II $\lambda 6355$ and Ca II H & K absorption when compared with spectra at the same phases as SN 1999aa. This effect is clearly seen in Figure 1 where the spectrum of SN 1999aa at -8 days is seen to be virtually identical to the spectrum of SN 1991T at -3 days. The trajectories of the CN SNe 1999ee and 2011fe are considerably more complex and different – not just with respect to SN 1991T and SN 1999aa, but also one from the other. Some of these differences are attributable to the presence of high-velocity Ca II at pre-maximum phases, which is particularly strong in SN 1999ee (see Figure 1 and Mazzali et al. 2005).

The pseudo equivalent widths for the Si II $\lambda 6355$ and Ca II H & K features were measured by defining a straight “continuum” level between the two flux peaks to either side of the absorption as illustrated in Figure 4 of Folatelli et al. (2013). Errors

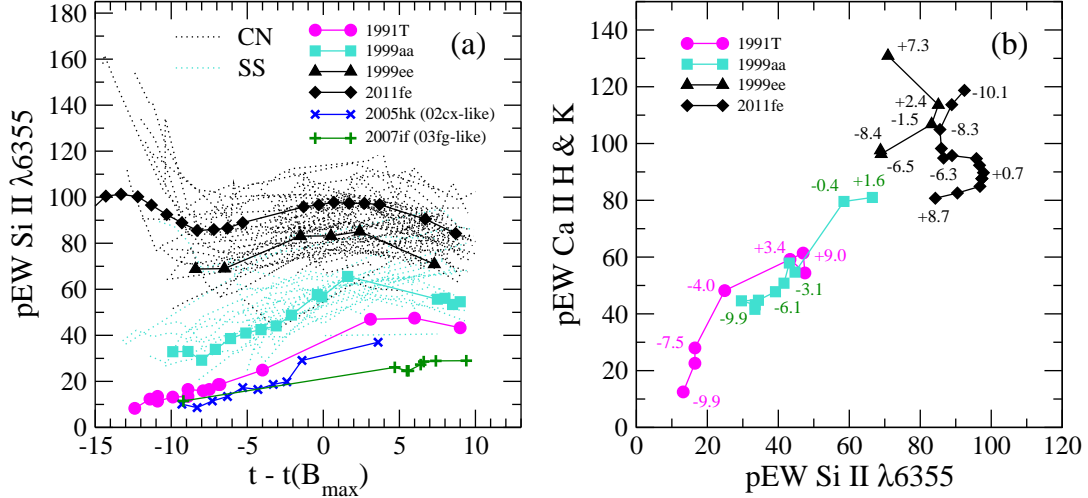


Figure 3. (a) Evolution of the pEW(Si II $\lambda 6355$) for SS (green dotted lines) and CN (black dotted lines) SNe from the Blondin et al. (2012) and Folatelli et al. (2013) spectroscopic samples. Measurements for SN 1991T, SN 1999aa, SN 1999ee, and SN 2011fe are highlighted. The spectra for SN 1991T are from Phillips et al. (1992) and Mazzali et al. (1995), those of SN 1999aa are from Garavini et al. (2004) and Blondin et al. (2012), those of SN 1999ee are from Hamuy et al. (2002b) and Blondin et al. (2012), and those of SN 2011fe are from Pereira et al. (2013). Also included are measurements for the 02cx-like SN2005hk, and for the 03fg-like event SN2007if. The spectra for SN2005hk are from Phillips et al. (2007) and Blondin et al. (2012), and those for SN2007if are from Scalzo et al. (2010) and Blondin et al. (2012).; (b) Evolution of the pseudo equivalent widths of the Ca II H & K and Si II $\lambda 6355$ absorption features as a function of light curve phase with respect to $t(B_{\max})$ for SN 1991T, SN 1999aa, SN 1999ee, and SN 2011fe. Each point in the diagram represents a spectrum, with a selection of the points labelled with the light curve phase.

estimated using the IRAF³ `splot` task were typical 20–30% for the weakest features and 5% or less for stronger lines. However, equivalent width measurements are susceptible to additional unaccounted errors in the subtraction of host galaxy light from the SN spectrum. This effect likely explains some of the “jaggedness” in the temporal evolution of the pEW(Si II $\lambda 6355$) measurements of the CN and SS SNe in Figure 3a. These errors can make it difficult in some cases to correctly separate 91T-like SNe from 99aa-like events.

In this paper, we use Figure 3a to identify true 91T-like SNe. However, certain peculiar SNe Ia can masquerade as 91T-like events if photometric information is not also available. In particular, the pre-maximum spectra of 02cx-like SNe (also known as “Type Iax” events; Foley et al. 2013) are likewise dominated by Fe III absorption lines, but at much lower expansion velocities than normal SNe Ia (Li et al. 2003). Figure 3 shows that the time evolution of the pEW(Si II $\lambda 6355$) measurements for the well-observed 02cx-like event, SN2005hk, closely mimic those of SN1991T. However, the 02cx-like events are sub-luminous compared to 91T-like SNe and, as opposed to 91T-like and normal SNe Ia, their i/I -band and NIR light curves peak

³ IRAF is distributed by the National Optical Astronomy Observatory, which is operated by the Association of Universities for Research in Astronomy (AURA) under cooperative agreement with the National Science Foundation.

after $t(B_{max})$ and do not show a secondary maximum (Li et al. 2003; Phillips et al. 2007; Ashall et al. 2020). Certain 03fg-like SNe⁴ can also display 91T-like spectra at pre-maximum phases, the best example being the well-studied SN2007if (Scalzo et al. 2010; Yuan et al. 2010). The evolution of pEW(Si II $\lambda 6355$) for SN2007if is also plotted in Figure 3a. Again, such objects can be discriminated from 91T-like SNe from their exceptionally broad i/I -band and NIR light curves that peak after $t(B_{max})$ and lack of a clear secondary maximum (Ashall et al. 2020, 2021).

To summarize, we employ both spectroscopic and photometric requirements for classifying a SN as a 91T-like event, which we define as follows:

- Spectroscopic: At least one pEW(Si II $\lambda 6355$) measurement before 10 days after B maximum that is consistent with the trajectory of SN 1991T in Figure 3a. In practical terms, this translates to $\text{pEW}(\text{Si II } \lambda 6355) < \sim 20 \text{ \AA}$ at $t - t(B_{max}) = -10 \text{ d}$, $< \text{than } \sim 40 \text{ \AA}$ at maximum, and $< \sim 50 \text{ \AA}$ at $t - t(B_{max}) = +10 \text{ d}$.
- Photometric: An i/I -band light curve that reaches maximum *before* the epoch of B maximum and displays a clear secondary maximum.

Before ending this section, it is important to emphasize that programs providing automated spectral classification such as SNID (Blondin & Tonry 2007) make little distinction between 91T-like and 99aa-like SNe. Indeed, the standard SNID template subgroups are “Ia-norm”, “Ia-91T”, “Ia-91bg”, “Ia-csm”, and “Ia-pec”. Hence, many SNe that SNID classifies as “Ia-91T” are actually “99aa-like” events.

3. 91T-LIKE SUPERNOVAE IN THE CSP-II SAMPLE

Using the above-described criteria, we have identified ten 91T-like events observed by the CSP-II. The CSP-II was carried out between 2011 October and 2015 May, during which high-quality optical and NIR light curves were obtained for 214 SNe Ia, 125 of which were located in the smooth Hubble flow at redshifts $0.027 < z < 0.137$ (Phillips et al. 2019). These data are being published separately in the final data release of CSP-II photometry (Suntzeff et al. 2022). Details concerning these ten 91T-like SNe are given in Appendix A, including plots of the temporal evolution of pEW(Si II $\lambda 6355$) and the individual light curves.

Selected optical spectra of the 91T-like SNe identified in the CSP-II sample are found in Figure 4. This figure illustrates that the spectra of events obtained at similar phases are quite similar overall. The largest differences are in the slopes (i.e., the colors) of the spectra, which are consistent with differences in host galaxy reddening. At pre-maximum epochs, the spectra are dominated by the Fe III $\lambda 4404$ and $\lambda 5129$ absorption features. Note, however, that the overall strengths of the Fe III lines can vary considerably from object to object. A prime example of this is illustrated in

⁴ These SNe are commonly referred to in the literature as “Super-Chandrasekhar” events. However, since the latter name presumes knowledge of the progenitors which, to date, has not been definitively proved, we will refer to them as “03fg-like” SNe, after the first recognized example (Howell et al. 2006).

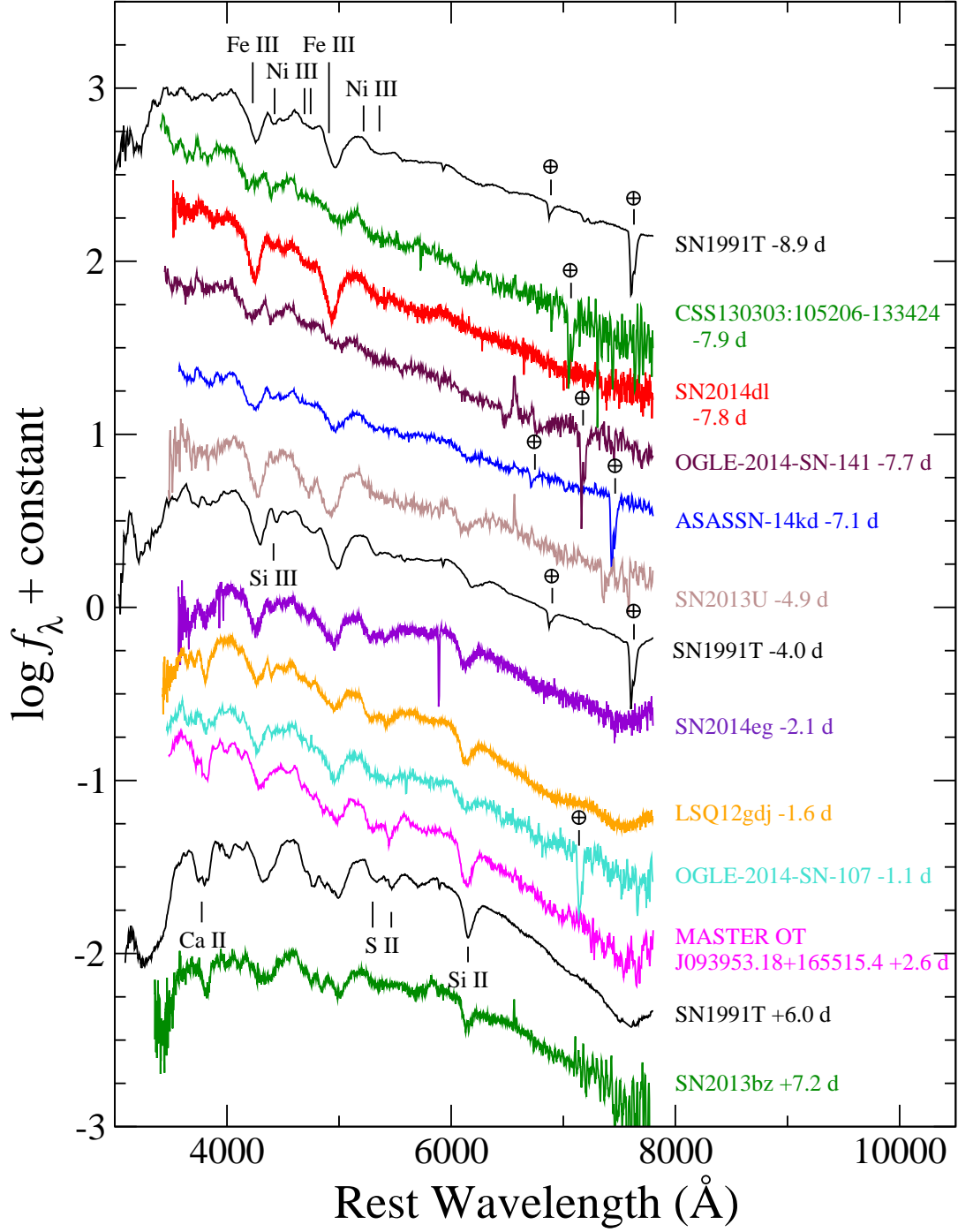


Figure 4. Optical spectra of the ten 91T-like SNe in the CSP-II sample obtained -8 to $+7$ days with respect to the time of maximum light in the B -band. Spectra of SN1991T at three phases covering this range are plotted in black for comparison. Where necessary, the spectra have been adjusted via a low-order polynomial to match the photometry. They have also been corrected for Galactic reddening using the [Schlafly & Finkbeiner \(2011\)](#) recalibration of the [Schlegel, Finkbeiner & Davis \(1998\)](#) infrared-based dust map and assuming $R_V = 3.1$. Unremoved telluric absorption features are marked with an \oplus symbol.

Figure 4, where the spectrum of SN2014dl is observed to have very strong Fe III absorption at -7.8 days, while these same lines are nearly washed out in the spectra

of CSS130303:105206-133424 at a phase of -7.9 days and OGLE-2014-SN-141 at -7.7 days. In between these two extremes is the spectrum of ASASSN-14kd obtained at -7.1 days. As noted by [Sasdehli et al. \(2014\)](#), the Fe III absorption observed at pre-maximum epochs in 91T-like SNe must be produced mostly by stable ^{54}Fe since ^{56}Co would not have had enough time since explosion to decay to ^{56}Fe . These authors concluded that the amount of stable Fe required to produce the observed Fe III absorption in SN 1991T is consistent with solar metallicity material in the progenitor. It is tempting to speculate that the observed variations in the strength of the Fe III absorption at pre-maximum epochs could reflect differences in the metallicities of the progenitors. It seems unlikely that this is an ionization effect since the strength of the Si III $\lambda 4564$ absorption (see below) shows less variation than Fe III $\lambda 4404$ in spite of the very similar ionization potentials of Fe^{++} and Si^{++} . And while differing amounts of host galaxy light contamination in the spectra might produce such variations, there is no evidence to support this, particularly in the case of CSS130303:105206-133424 which exploded in the outer region of its faint host.

Other weaker absorption features visible between and redward of the Fe III $\lambda\lambda 4404, 5129$ lines at these early phases (see top panel of Figure 1) have been ascribed to transitions of Ni III ([Ruiz-Lapuente et al. 1992](#); [Mazzali et al. 1995](#); [Fisher et al. 1999](#); [Hatano et al. 2002](#)). The -8.9 days spectrum of SN 1991T plotted in Figure 4 shows a strong absorption feature at 3200 \AA which, according to [Sasdehli et al. \(2014\)](#), is a blend of Co III and Fe III lines, with the Co arising from the decay of ^{56}Ni . These authors concluded that Ni, Co, and Fe must be present to velocities as high as $\sim 17,000 \text{ km s}^{-1}$ to match the shape of the spectral features produced by these elements.

Absorption due to multiplet 2 of Si III ($\lambda_0 \simeq 4564 \text{ \AA}$) is present in the pre-maximum spectra of 91T-like events beginning at the earliest epochs ([Jeffery et al. 1992](#); [Mazzali et al. 1995](#)). However, Si II $\lambda 6355$ absorption does not become clearly visible until approximately a week before maximum light, and Ca II H & K and the iconic “W” absorption feature of S II at $\sim 5400 \text{ \AA}$ are undetectable until only a few days before maximum light. The presence of Si III absorption early on demonstrates that intermediate-mass elements are present in the outermost layers of 91T-like SNe, but are largely invisible due to the unusually high radiation temperatures at these phases ([Mazzali et al. 1995](#); [Nugent et al. 1995](#); [Sasdehli et al. 2014](#)). This may also account for the lack of observable high-velocity Ca II and Si II in the outer ejecta of 99aa-like and 91T-like SNe.

As mentioned in §1 and illustrated in the bottom panel of Figure 1, by two weeks after maximum, the optical spectra of 91T-like SNe begin to closely resemble those of normal SNe Ia. P-Cygni lines of Ca II H & K and the $\lambda\lambda 8498, 8542, 8662$ triplet are clearly visible, and Fe II features begin to dominate much of the spectrum (e.g., see Figure 10 of [Jeffery et al. 1992](#)). Broad absorption is present at $\sim 7500 \text{ \AA}$ (see Figure 5 of [Filippenko et al. 1992](#)) which several authors have identified with O I $\lambda 7774$

(Filippenko et al. 1992; Jeffery et al. 1992; Sasdelli et al. 2014). Unfortunately, at these phases, the strength of the Si II absorption is no longer a useful tool for separating 91T-like events from 99aa-like and slow-declining Branch CN SNe.

4. ABSOLUTE MAGNITUDES

As highlighted in the introduction to this paper, and also summarized by Taubenberger (2017) in his review article, 91T-like SNe have long been suspected of being intrinsically brighter than “normal” SNe Ia at the luminous end of the absolute magnitude versus decline rate relation. In the case of SN 1991T itself, if we assume the Cepheid-based distance modulus of 30.74 ± 0.12 (statistical) ± 0.12 (systematic) measured by Saha et al. (2001) and use the SNOOPy EBV_model2 (Burns et al. 2011) to fit the *UBVRI* photometry published by Lira et al. (1998), a host reddening of $E(B - V) = 0.15 \pm 0.01$ mag and an absolute magnitude of $M_V = -19.62 \pm 0.22$ are implied. This is 0.23 ± 0.23 mag brighter than a SN with $s_{BV} = 1.1$ ⁵ according to the M_V versus s_{BV} relation for SNe Ia given by Burns et al. (2018) for events with $s_{BV} > 0.5$ and $E(B - V)_{\text{host}} < 0.5$ mag. While interesting, the large error in this measurement does not allow a definitive conclusion. A better approach would be to compare a sample of 91T-like SNe in the smooth Hubble flow where the redshift can be used as a precise relative measurement of distance. The CSP-II sample of SNe Ia provides such an opportunity.

In Figure 5, we plot Hubble diagram residuals, $\Delta(m - M)$, versus $\Delta m_{15}(B)$ for the 91T-like and 99aa-like SNe observed by the CSP-II. The Hubble diagram residual is defined as the difference between the distance modulus predicted from the host galaxy redshift using a best-fit cosmological model⁶ to the full set of SNe Ia observed by the CSP-I and CSP-II, and the distance modulus derived from the intrinsic color analysis described in detail by Burns et al. (2018). For comparison, the Hubble diagram residuals for the slow-declining Branch CN SNe in the CSP-II sample, which we define as those events with $\Delta m_{15}(B) < 1.10$, are also plotted in Figure 5. Negative values therefore indicate more luminous SNe Ia. This figure clearly shows that all of the 91T-like SNe have negative Hubble diagram residuals, implying that they are over-luminous by ~ 0.1 – 0.5 mag. It also confirms that 91T-like (and 99aa-like) SNe cannot be distinguished from slow-declining Branch CN events with similar decline rates on the basis of their $\Delta m_{15}(B)$ measurements alone.

To separate the 91T-like events from the 99aa-like and slow-declining Branch CN SNe, Hubble diagram residuals are plotted versus $\text{pEW}(\text{Si II } \lambda 6355)$ at maximum light in Figure 6. The $\text{pEW}(\text{Si II } \lambda 6355)$ values for the 99aa-like and slow-declining Branch CN SNe are taken from Morrell et al. (2022), while for the 91T-like SNe, a low-order polynomial fit to the shape of the evolution of the equivalent width values

⁵ The color stretch parameter, s_{BV} , is a dimensionless parameter defined as the time difference between *B*-band maximum and the reddest point in the $(B - V)$ color curve divided by 30 days, where typical SNe Ia have $s_{BV} \sim 1$ (Burns et al. 2014).

⁶ Assumes standard Λ CDM cosmology and a fixed Hubble constant $H_0 = 72 \text{ km s}^{-1} \text{ Mpc}^{-1}$, density parameter $\Omega_m = 0.27$, and cosmological constant parameter $\Omega_\Lambda = 0.73$.

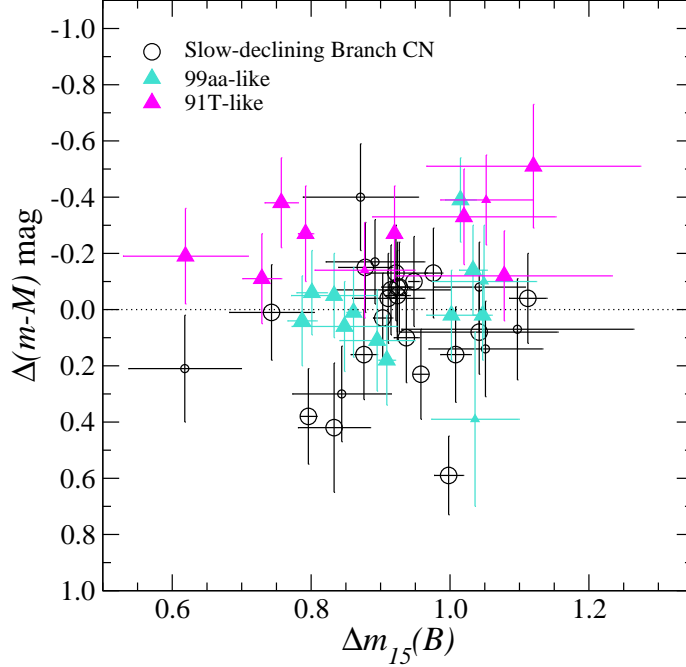


Figure 5. Hubble diagram distance modulus residuals, $\Delta(m - M)$, for 91T-like, 99aa-like, and slow-declining Branch CN SNe observed by the CSP-II. The sample of slow-declining Branch CN SNe is defined as those events with $\Delta m_{15}(B) < 1.10$. The larger symbols are SNe whose values of $\Delta m_{15}(B)$ were measured directly; the smaller symbols correspond to those where SNooPy template fits were used to measure the decline rate. The samples were limited to those with redshifts $z \geq 0.02$ to minimize uncertainties due to peculiar velocities. Note that negative values of $\Delta(m - M)$ correspond to overluminous events.

for SN 1991T was used to extrapolate the pEW measurements to maximum light. The error bars reflect the average error obtained in applying the same extrapolation method to the individual measurements of pEW(Si II $\lambda 6355$) for SN 1991T. Again, we see that the distance modulus residuals of the 99aa-like and Branch CN SNe scatter about zero, whereas the values for the 91T-like SNe are systematically negative.

As will be presented in a future paper, the $(B - v)$ and $(r - i)$ colors of the 91T-like SNe at maximum light appear to be similar to those of the 99aa-like and slow-declining Branch CN SNe. Nevertheless, the possibility must be considered that the apparent overluminous nature of the 91T-like events is the result of overestimates of the effect of host galaxy reddening due to incorrect assumptions of the colors of these extreme SNe. In the lower half of Figure 6 we plot the $E(B - V)_{\text{host}}$ values returned by SNooPy for the SNe plotted in the upper half of this figure. The mean host reddening for the 91T-like SNe is ~ 0.06 mag higher than the average values for the 99aa-like and slow-declining Branch CN events (see Table 1). Two of the four most luminous 91T-like objects, SN 2013U and SN 2013bz, have relatively large values of $E(B - V)_{\text{host}}$ (0.20 ± 0.02 and 0.23 ± 0.02 mag, respectively). However, the two others, OGLE-2014-SN-107 and SN 2014dl, have more modest values of $E(B - V)_{\text{host}} = 0.13 \pm 0.03$ mag and 0.05 ± 0.01 mag.

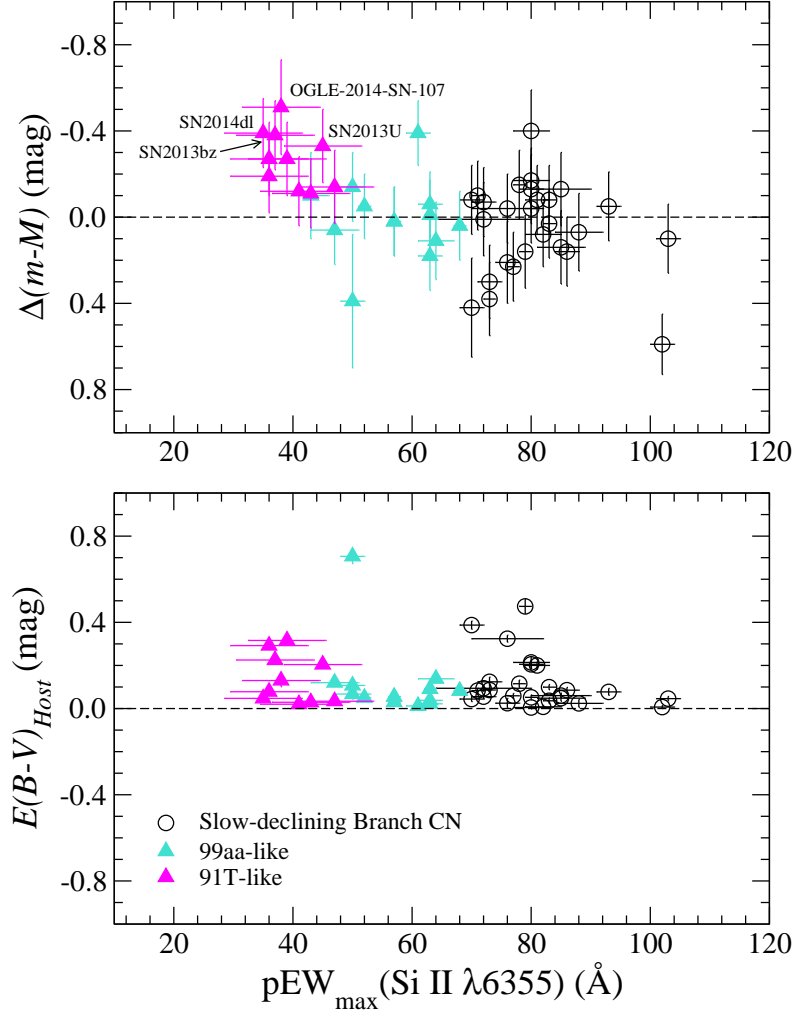


Figure 6. (above) Hubble diagram residuals in magnitudes plotted versus the pseudo equivalent width of the Si II $\lambda 6355$ absorption at maximum light for 91T-like, 99aa-like, and CN SNe observed by the CSP-II. (below) $E(B - V)_{\text{host}}$ values derived using `SNooPy` for the same SNe.

A way of checking whether errant host galaxy dust corrections are responsible for the systematically-higher luminosities of the 91T-like SNe compared to the 99aa-like and slow-declining Branch CN events is to look at the Hubble diagram residuals as a function of wavelength. In particular, we would expect dust absorption to have a much smaller effect on the Hubble diagram residuals for the NIR filters compared to the optical. The values of $\Delta(m - M)$ plotted in the upper half of Figure 6 are derived from combining the `SNooPy` fits to the $uBgVriYJH$ light curves. However, we can also look at the residuals as a function of the individual filters. Table 1 indicates that the weighted mean Hubble diagram residuals for the 91T-like, 99aa-like, and CN samples are remarkably constant from the optical to the NIR. This is displayed graphically in Figure 7 where the residuals in V , r , Y , and H for each SN are plotted versus the residuals in B . Excellent correlations are observed in all four bands, with the 91T-like SNe consistently occupying the most-luminous part.

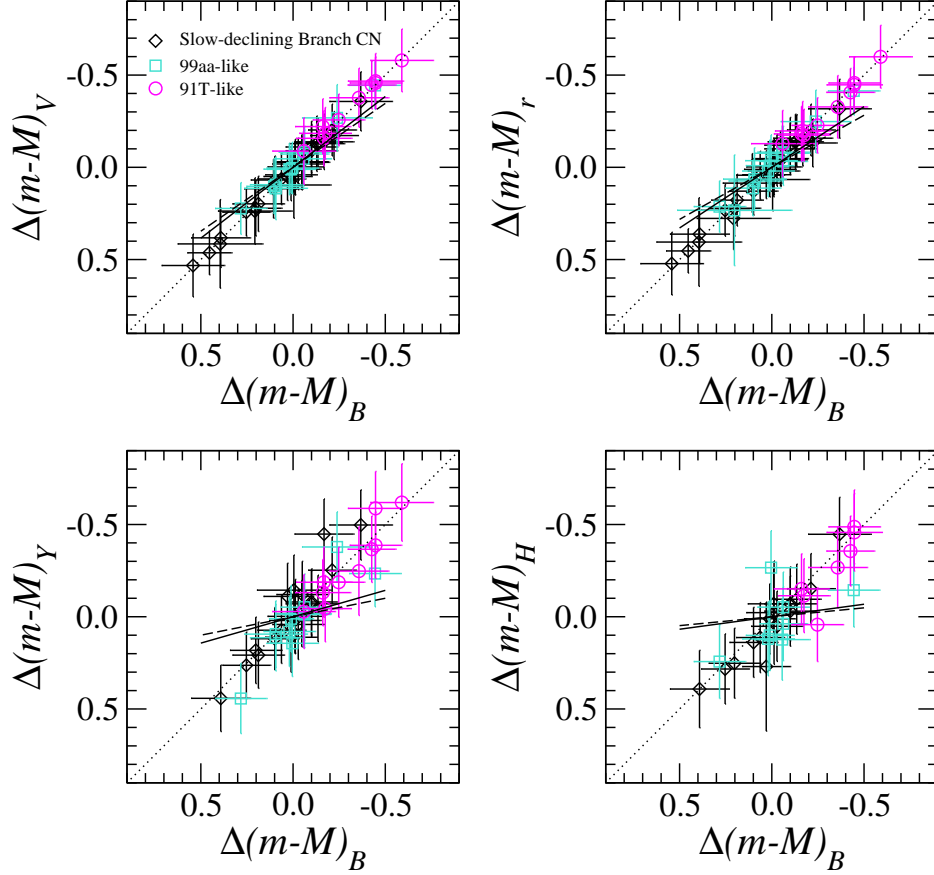


Figure 7. B -band Hubble diagram residuals in magnitudes plotted versus the residuals in V , r , Y , and H for 91T-like, 99aa-like, and and CN SNe observed by the CSP-II. The solid black line in each plot indicates the expected correlation in the residuals for $R_V = 3$ and a systematic error between ± 0.5 mag in $E(B - V)$; the dashed black line shows the same for $R_V = 2$.

Table 1. Mean values of $\Delta m_{15}(B)$, $E(B - V)_{host}$, and $\Delta(m - M)$ for CSP-II SNe Ia

Parameter	91T-like	n	SS	n	CN	n
$\Delta m_{15}(B)$	0.87 (0.17)	10	0.92 (0.11)	13	0.92 (0.10)	27
$E(B - V)_{host}$	0.12 (0.11)	10	0.07 (0.19)	13	0.06 (0.13)	27
$\Delta(m - M)_B$	-0.31 (0.18)	10	-0.01 (0.19)	13	+0.04 (0.22)	27
$\Delta(m - M)_V$	-0.33 (0.16)	10	-0.03 (0.19)	13	+0.05 (0.22)	27
$\Delta(m - M)_r$	-0.32 (0.16)	10	-0.03 (0.18)	13	+0.05 (0.21)	27
$\Delta(m - M)_Y$	-0.27 (0.21)	10	+0.02 (0.21)	11	-0.01 (0.22)	20
$\Delta(m - M)_H$	-0.25 (0.19)	7	+0.02 (0.17)	8	+0.03 (0.21)	15
$\Delta(m - M)_{uBgVrYJH}^a$	-0.33 (0.18)	10	-0.01 (0.15)	13	+0.05 (0.22)	27

NOTE—All values shown are weighted means. The root mean square dispersion is given in parentheses, followed by the number of SNe, “n”, used in calculating the mean.

^a Average cross-validated distance modulus calculated from the u , B , g , V , r , i , Y , J , and H filters (see Burns et al. 2018)

The `SNooPy color_model` method used to calculate the Hubble diagram residuals in Table 1 and Figures 5–7 employs intrinsic colors from Burns et al. (2018) to constrain $E(B - V)$ and R_V for each SN. These values, in turn, are used to compute reddening-corrected magnitudes. Errors in $E(B - V)$ and R_V will therefore propagate a systematic error in the Hubble diagram residual in all filters. However, such errors should grow smaller with wavelength (see Figure 7) and cannot account for the strong, slope = 1, correlations observed in Figure 7 which are dominated by the peculiar velocities of the host galaxies. Moreover, except for OGLE-2014-SN-141, the `color_model` method gives acceptable fits in the *BVriYJH* bands (see Appendix A). Still, it is important to confirm that the high luminosities of 91T-like SNe in all filters are not an artifact of the `color_model` method. The Hubble diagram residuals for CSP-II SNe Ia published by Uddin et al. (2022) provide an alternative check since these were derived by applying the empirical Tripp (1998) luminosity–color relation to maximum light magnitudes derived from the `SNooPy max_model` method. This analysis yields average residuals in *all* filters of approximately -0.22 ± 0.07 mag, -0.04 ± 0.05 mag, and $+0.08 \pm 0.04$ mag for the 91T-like, 99aa-like, and slow-declining Branch CN SNe, respectively, confirming that 91T-like SNe are systematically more luminous than their 99aa-like and slow-declining Branch CN counterparts. Figures 5–7, as well as Table 1, also suggest that 99aa-like SNe may be intermediate in luminosity between 91T-like and slow-declining Branch CN events, but this will require future confirmation from larger samples.

5. CONCLUSIONS

91T-like SNe are the extreme members of the Branch SS group in displaying the weakest Si II $\lambda 6355$ and Ca II H & K absorption at maximum light of any SNe Ia. We show that these objects can be identified from one or more optical spectra by plotting $pEW(\text{Si II } \lambda 6355)$ versus light curve phase for $t - t(B_{max}) \leq +10$ days. They are differentiated from 02cx-like and 03fg-like SNe in possessing *i/I*-band light curves that reach maximum before the of epoch *B* maximum, and that also display a clear secondary maximum. Lacking accurate knowledge of light curve phase, 91T-like SNe may be easily confused with the less extreme 99aa-like events.

From a sample of ten 91T-like SNe observed during the course of the CSP-II, we find clear evidence that 91T-like SNe are over-luminous by ~ 0.1 – 0.5 mag compared to 99aa-like and slow-declining Branch CN SNe. This difference in luminosity is remarkably constant from optical to NIR wavelengths, arguing that overestimates of the host galaxy dust corrections cannot explain this finding. The data further suggest that 99aa-like events may be intermediate in luminosity between 91T-like SNe and slow-declining Branch CN SNe, although this requires further confirmation.

Based on an analysis by Leaman et al. (2011) of 726 SNe discovered by the Lick Observatory Supernova Search (LOSS), Li et al. (2011) concluded that 9% of all SNe Ia

in the local Universe are 91T-like events. However, Li et al. employed a broad definition for what constituted a “Ia 91T” that included 99aa-like events. In any event, they are likely to be sufficiently rare in the local Universe that their effect on measurements of the Hubble constant should be small. This is borne out by an analysis of the CSP-II sample using the methodology of Uddin et al. (2022). Restricting the sample to the 178 SNe Ia with $s_{BV} > 0.8$ so as to exclude lower-luminosity events, and then repeating the calculation after removing the ten 91T-like events, the value of the Hubble constant changes by only 0.1%. However, there is no assurance that the frequency of 91T-like remains constant at greater and greater look-back times. And even if their relative numbers have not changed as the Universe has evolved, we can expect to observe proportionately more of them at the magnitude limits of discovery surveys due to Malmquist bias. Unfortunately, the light curve width alone cannot be used to identify 91T-like SNe, although this may not be true at ultraviolet wavelengths (Jiang et al. 2018). At least for now, spectroscopy combined with rest frame i/I -band photometry remains the most reliable tool for discriminating between 91T-like, 99aa-like, and slow-declining Branch CN SNe.

1 The work of the CSP-II has been generously supported by the National Science Foun-
2 dation under grants AST-1613426, AST-1613455, and AST-1613472. The CSP-II was
3 also supported in part by the Danish Agency for Science and Technology and Inno-
4 vation through a Sapere Aude Level 2 grant. M. Stritzinger acknowledges funding
5 by a research grant (13261) from VILLUM FONDEN. E.B. is supported in part
6 by NASA grant 80NSSC20K0538. L.G. acknowledges financial support from the
7 Spanish Ministerio de Ciencia e Innovación (MCIN), the Agencia Estatal de Investi-
8 gación (AEI) 10.13039/501100011033, and the European Social Fund (ESF) ”Invest-
9 ing in your future” under the 2019 Ramón y Cajal program RYC2019-027683-I and
10 the PID2020-115253GA-I00 HOSTFLOWS project, from Centro Superior de Inves-
11 tigaciones Científicas (CSIC) under the PIE project 20215AT016, and the program
12 Unidad de Excelencia María de Maeztu CEX2020-001058-M. We gratefully acknowl-
13 edge the use of WISEREP – <https://wiserep.weizmann.ac.il>. M.M.P. thanks Richard
14 Scalzo for interesting discussions of extreme SNe Ia. This research has made use of
15 the NASA/IPAC Extragalactic Database (NED), which is funded by the National
16 Aeronautics and Space Administration and operated by the California Institute of
17 Technology. Finally, we thank the referee for suggestions on improving the text and
18 figures.

Facilities: Magellan:Baade (IMACS imaging spectrograph, FourStar wide-field near-infrared camera, Magellan:Clay (LDSS3 imaging spectrograph), Swope (SITe3 CCD imager, e2v 4K x 4K CCD imager), du Pont (SITe2 CCD imager, Tek5 CCD imager, WFCCD imaging spectrograph, RetroCam near-infrared imager), NOT (AL-

FOSC), La Silla-QUEST, CRTS, PTF, iPTF, OGLE, ASAS-SN, PS1, KISS, ISSP, MASTER, SMT)

Software: IRAF([Tody 1986, 1993](#)), SNooPy ([Burns et al. 2011](#))

APPENDIX

A. 91T-LIKE SNE FROM THE CSP-II

A total of ten 91T-like events in the CSP-II sample were identified using the spectroscopic and photometric criteria defined in §2. These objects are listed in Table A1. Figure A1 shows the temporal evolution of $pEW(\text{Si II } \lambda 6355)$ for the CSP-II sample, and, in Figures A2–A4, `SNooPY color_model` fits are plotted. These fits employ the intrinsic colors from Burns et al. (2018) to constrain $E(B - V)$ and R_V for each SN.

Comments on individual objects are as follows:

- LSQ12gdj: Extensive observations of this SN have been previously published by Scalzo et al. (2014), who concluded that it was “spectroscopically 91T-like”. Figure A1 shows that the evolution of the pseudo equivalent width of Si II $\lambda 6355$ was more similar to SN 1991T than SN 1999aa. The light curves plotted in Figure A3 also clearly show that LSQ12gdj had a strong secondary maximum in the i band, and that primary maximum in i was reached before B maximum.
- SN 2013U: This SN was discovered by the Puckett Observatory Supernova Search⁷ and was correctly classified as a 91T-like event from a spectrum obtained with the Asiago 1.82-m Copernico Telescope (Gagliano et al. 2013; Tomasella et al. 2013). The `SNooPy color_model` templates displayed in Figure A3 provide excellent fits at maximum light in the $BVgri$ filters, but underpredict the observed brightness in u . Comparing with the other SNe with u -band photometry plotted in Figure A3, this appears to be a general characteristic of 91T-like SNe (see also Scalzo et al. 2014).
- CSS130303:105206-133424: This object was discovered by the Catalina Real-Time Transient Survey (CRTS; Djorgovski et al. 2011). A spectrum obtained by the Public ESO Spectroscopic Survey of Transient Objects (PESSTO; Smartt et al. 2015) with the ESO La Silla 3.6 m NTT was classified by Blagorodnova et al. (2013) as corresponding to a SN Ia caught ~ 7 days before maximum light. As discussed in §3, this spectrum is peculiar even for a 91T-like event in showing only very weak absorption features, including those of Fe III.
- MASTER OT J093953.18+165516.4: The discovery of this SN by the MASTER network of robotic telescopes (Gorbovskoy et al. 2013) was announced by Shumkov et al. (2013). It was independently discovered by the CRTS with the designation MLS130215:093953+165516. A PESSTO spectrum obtained by Benitez-Herrera et al. (2013) was stated to show “similarity with that of the

⁷ <http://www.cometwatch.com/supernovasearch.html>

peculiar, 1991T-like SN 1998es” near maximum light. SN 1998es was actually a 99aa-like event according to the classification method presented in §2. However, as seen in Figure A1, measurement of $pEW(\text{Si II } \lambda 6355)$ from this spectrum of MASTER OT J093953.18+165516.4 is consistent with a 91T-like event a few days after maximum light. Technically speaking, the CSP-II *i*-band photometry plotted in Figure A3 does not begin early enough to confirm that maximum was reached before maximum light in *B*, but the excellent fits to the SNOOPy templates leave little doubt that this was a bonafide 91T-like SN.

- SN 2013bz: This is another SN discovered by the CRTS (Howerton et al. 2013) which designated it as SNhunt188. A spectrum taken with the Asiago 1.82-m Copernico Telescope by Ochner et al. (2013) was said to be “a good match ... with the so-called ‘super-Chandrasekhar’ SNe Ia 2006gz and 2009dc.” However, a spectrum obtained 4 days earlier with the 4.2-m William Herschel Telescope by Chen et al. (Howerton et al. 2013) was stated to be consistent with either a normal SN Ia at maximum light, or a 91T-like event a week after maximum. The CSP-II light curves indicate that this spectrum, which is not publicly available, was obtained at +3 days. The value of $pEW(\text{Si II } \lambda 6355)$ measured from the Asiago spectrum is fully consistent with a 91T-like classification (see Figure A1). This SN has a striking excess at *u*-band maximum (see Figure A3).
- SN 2014dl: Yet another SN discovered by the CRTS (Drake et al. 2014). Spectra obtained at the Asiago and Las Campanas Observatories were found to be similar to that of a 91T-like event ~ 1 week before maximum (Drake et al. 2014).
- OGLE-2014-SN-107: This object was discovered in the course of the OGLE-IV Real-Time Transient Search (Wyrzykowski et al. 2014). From a PESSTO spectrum, Takats et al. (2014) classified it as a 91T-like SN observed approximately ~ 5 days before maximum light. This is confirmed in Figure A1. As illustrated in Figure A3, the minimum between the primary and secondary maxima of the *i*-band light curve of this SN is particularly shallow.
- ASASSN-14kd: The discovery of this SN in the course of the All-Sky Automated Survey for Supernovae (ASASSN) (Shappee et al. 2014; Kochanek et al. 2017) was announced by (Nicholls et al. 2014). From a PESSTO spectrum obtained within hours of discovery, Firth et al. (2014) identified it as a SN Ia that was best matched by SNID 91T-like templates at a phase of -7 days, which we confirm in Figure A1.
- OGLE-2014-SN-141: This is another SN discovered by the OGLE-IV Real-Time Transient Search. A single PESSTO spectrum was obtained by Dimitriadis et al. (2014), who classified it as a SN Ia at a phase of approximately -7 days and noted that it was an “excellent match to a SN1991T-like

SN Ia.” This is confirmed in Figure A1. Interestingly, although the `SNooPy` `color_model` gives a good fit to the *BVRi* light curves with a host galaxy color excess of 0.08 ± 0.02 mag and $R_V = 3.4 \pm 0.9$, the *Y* and *J* templates over predict the brightness in the NIR by ~ 0.4 – 0.6 mag.

- SN2014eg: This SN was serendipitously discovered in ESO 154-G010 by PESSTO observers who were obtaining follow-up observations of the Type II-n SN 2013fc in the same host galaxy. A spectrum was obtained six nights later by Smith et al. (2014) who classified SN2014eg as a 91T-like caught approximately one week before maximum. Extensive spectroscopic and photometry observations of this SN may be found in Dimitriadis (2017).

Table A1. 91T-like Supernovae Observed by the CSP-II

SN Name	Host Galaxy	z_{helio}^a	$\Delta m_{15}(B)^b$	s_{BV}^c	Spectroscopy ^d
LSQ12gdj	ESO 472-G 007	0.0303	0.73 (0.03)	1.14 (0.05)	1
SN2013U	CGCG 008-023	0.0345	1.02 (0.13)	1.25 (0.05)	2,3,4
CSS130303:105206-133424	GALEXASC J105206.27-133420.2	0.0789	1.08 (0.16)	1.19 (0.05)	5
MASTER OT J093953.18+165516.4	CGCG 092-024	0.0478	0.84 (0.04)	1.12 (0.05)	6
SN2013bz (SNhunt188)	2MASX J13265081-1001263	0.0192	0.76 (0.02)	1.12 (0.05)	4,7
SN2014dl (CSS140925:162946+083831)	UGC 10414	0.0330	1.05 (0.07)*	1.22 (0.05)	3,4,8,9
OGLE-2014-SN-107	APMUKS(BJ) B004021.02-650219.5	0.0664 ^e	1.12 (0.05)	1.19 (0.05)	10
ASASSN-14kd	2MASX J22532475+0447583	0.0243 ^e	0.79 (0.01)	1.13 (0.05)	3,11
OGLE-2014-SN-141	2MASX J05371898-7543157	0.0625 ^e	0.62 (0.09)	1.24 (0.05)	12
SN2014eg	ESO 154-G 010	0.0186	0.92 (0.01)	1.17 (0.05)	3,4

^a Heliocentric redshift are from the NASA/IPAC Extragalactic Database (NED) unless otherwise indicated.

^b $\Delta m_{15}(B)$ decline rate in magnitudes (Phillips 1993) as measured with `SNooPy`. The 1σ error is given in between parentheses. The * symbol indicates values derived from template fits only.

^c s_{BV} color stretch (Burns et al. 2014) as measured with `SNooPy` templates. The 1σ error is given in between parentheses.

^d References to spectroscopic observations.

^e Redshift measured by CSP-II.

References— (1) Scalzo et al. (2014); (2) Tomasella et al. (2013); (3) This paper; (4) PESSTO; (5) Blagorodnova et al. (2013); (6) Benitez-Herrera et al. (2013); (7) Ochner et al. (2013); (8) Drake et al. (2014); (9) Stahl et al. (2020) (10) Takats et al. (2014); (11) Firth et al. (2014); (12) Dimitriadis et al. (2014)

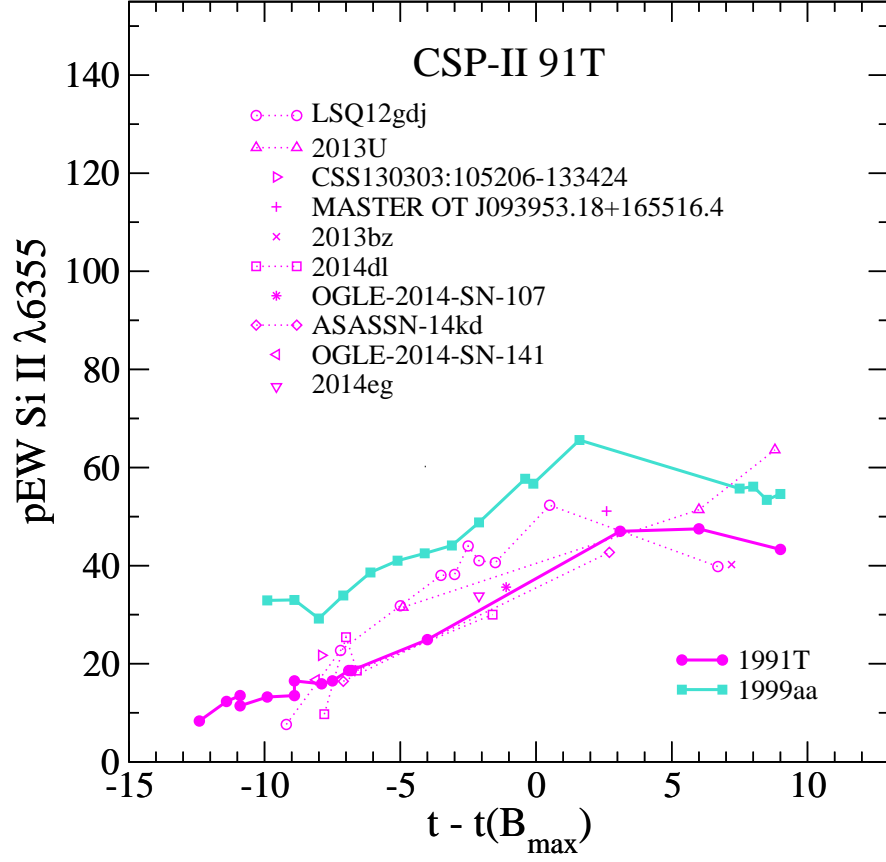


Figure A1. Evolution of pEW(Si II λ 6355) for 91T-like SNe identified in the CSP-II sample. The trajectories of SN 1991T and SN 1999aa in this diagram are plotted for reference.

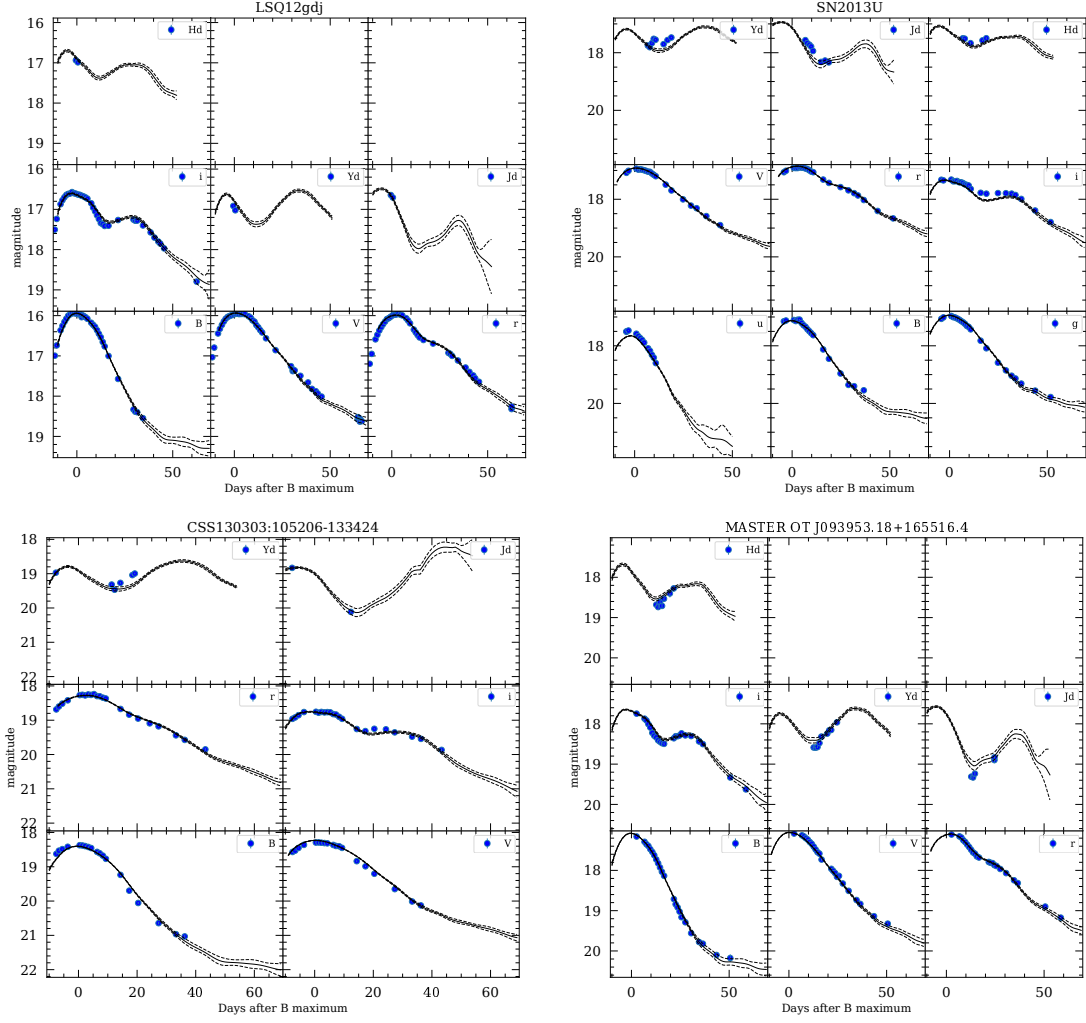


Figure A2. SNooPy fits to the 91T-like SNe LSQ12gdj, SN2013U, CSS130303:105206-133424, and SN 2014eg derived using the intrinsic color analysis described by Burns et al. (2018). Magnitudes plotted on the y-axis for each filter are as observed. The x-axis gives the time in days *in the observer frame* after the epoch of *B* maximum.

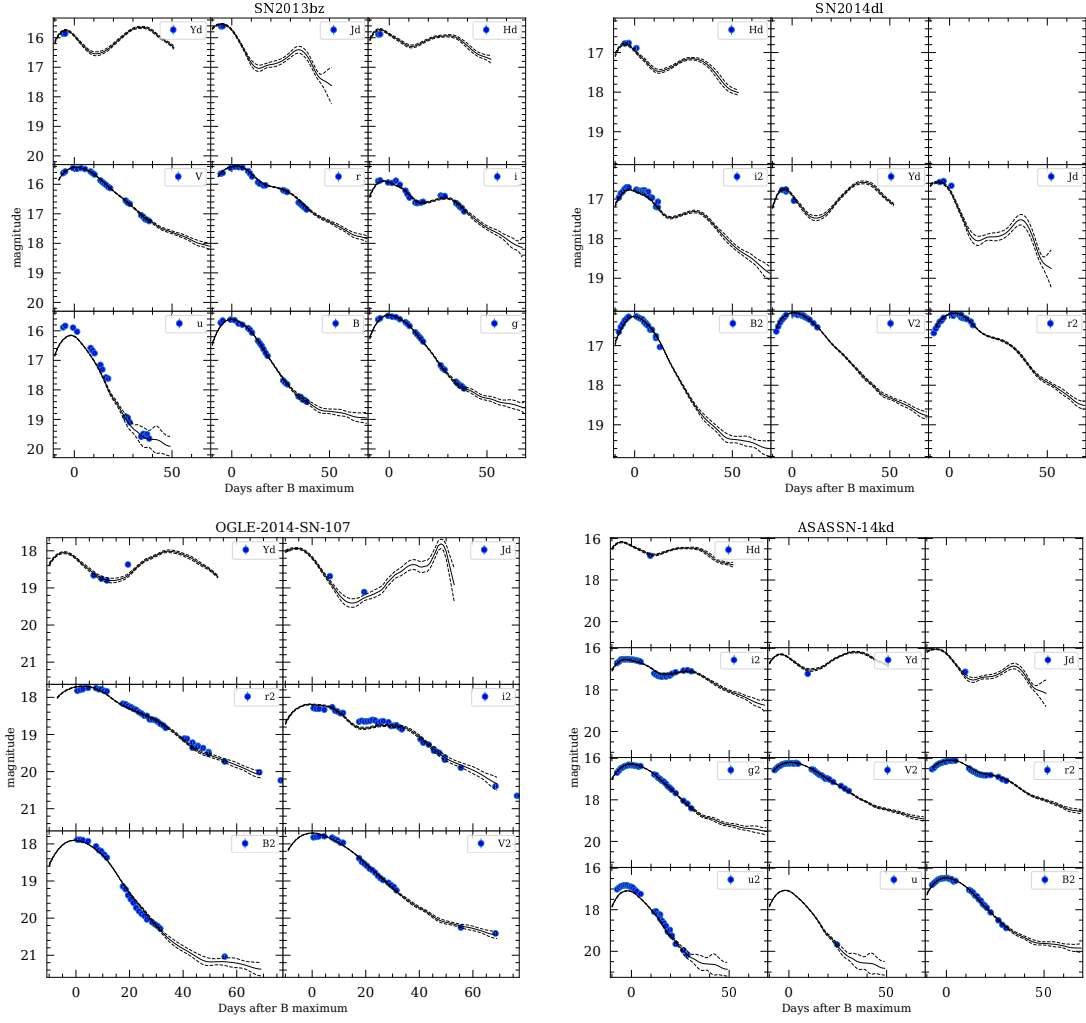


Figure A3. Same as Figure A2, except for the 91T-like SNe 2013bz, 2014dl, OGLE-2014-SN-107, and ASASSN-14kd.

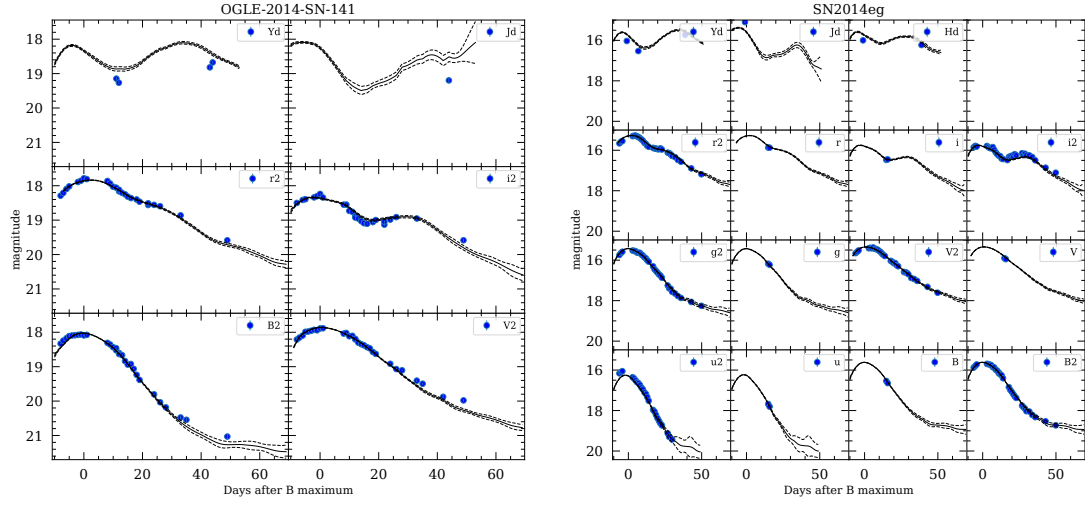


Figure A4. Same as Figure A2, except for the 91T-like SNe OGLE-2014-SN-141 and SN 2014eg.

REFERENCES

- Aldering, G., Antilogus, P., Bailey, S., et al. 2006, *ApJ*, 650, 510
- Ashall, C., Hsiao, E. Y., Hoefflich, P., et al. 2019, *ApJL*, 875, L14
- Ashall, C., Lu, J., Burns, C., et al. 2020, *ApJL*, 895, L3
- Ashall, C., Lu, J., Hsiao, E. Y., et al. 2021, *ApJ*, 922, 205
- Avelino, A., Friedman, A. S., Mandel, K. S., et al. 2019, *ApJ*, 887, 106
- Benitez-Herrera, S., Taubenberger, S., Garoffolo, A. M., et al. 2013, *The Astronomer's Telegram*, 4801
- Blagorodnova, N., Nicholl, M., Walton, N., et al. 2013, *The Astronomer's Telegram*, 4852
- Blondin, S., Matheson, T., Kirshner, R. P., et al. 2012, *AJ*, 143, 126
- Blondin, S., & Tonry, J. L. 2007, *ApJ*, 666, 1024
- Branch, D. 2001, *PASP*, 113, 169
- Branch, D., Chau Dang, L., & Baron, E. 2009, *PASP*, 121, 238
- Branch, D., Dang, L. C., Hall, N., et al. 2006, *PASP*, 118, 560
- Burns, C. R., Parent, E., Phillips, M. M., et al. 2018, *ApJ*, 869, 56
- Burns, C. R., Stritzinger, M., Phillips, M. M., et al. 2011, *AJ*, 141, 19
- Burns, C. R., Stritzinger, M., Phillips, M. M., et al. 2014, *ApJ*, 789, 32
- Burrow, A., Baron, E., Ashall, C., et al. 2020, *ApJ*, 901, 154
- Dhawan, S., Jha, S. W., & Leibundgut, B. 2018, *A&A*, 609, A72
- Dilday, B., Howell, D. A., Cenko, S. B., et al. 2012, *Science*, 337, 942
- Dimitriadis, G. 2017, Ph.D. thesis, University of Southampton
- Dimitriadis, G., Smith, M., Firth, R., et al. 2014, *The Astronomer's Telegram*, 6706
- Djorgovski, S. G., Drake, A. J., Mahabal, A. A., et al. 2011, *arXiv:1102.5004*
- Drake, A. J., Djorgovski, S. G., Graham, M. J., et al. 2014, *Central Bureau Electronic Telegrams* 3995, 1
- Filippenko, A. V., Li, W. D., & Leonard, D. C. 1999, *IAUC*, 7108, 2
- Filippenko, A. V., Richmond, M. W., Matheson, T., et al. 1992, *ApJL*, 384, L15
- Firth, R., Dimitriadis, G., Smith, M., et al. 2014, *The Astronomer's Telegram*, 6699
- Fisher, A., Branch, D., Hatano, K., & Baron, E. 1999, *MNRAS*, 304, 67
- Folatelli, G., Morrell, N., Phillips, M. M., et al. 2013, *ApJ*, 773, 53
- Foley, R. J., Challis, P. J., Chornock, R., et al. 2013, *ApJ*, 767, 57
- Freedman, W. L., Madore, B. F., Hatt, D., et al. 2019, *ApJ*, 882, 34
- Gagliano, R., Newton, J., Puckett, T., et al. 2013, *Central Bureau Electronic Telegrams*, 3410
- Garavini, G., Aldering, G., Amadon, A., et al. 2005, *AJ*, 130, 2278
- Garavini, G., Folatelli, G., Goobar, A., et al. 2004, *AJ*, 128, 387
- Gómez, G., López, R., & Sánchez, F. 1996, *AJ*, 112, 2094
- Gorbovskey, E. S., Lipunov, V. M., Kornilov, V. G., et al. 2013, *Astronomy Reports*, 57, 233
- Graham, M. L., Harris, C. E., Nugent, P. E., et al. 2019, *ApJ*, 871, 62
- Hachinger, S., Mazzali, P. A., Tanaka, M., et al. 2008, *MNRAS*, 389, 1087
- Hamuy, M., Maza, J., Pinto, P. A., et al. 2002, *AJ*, 124, 417 [Erratum: 2002, *AJ*, 124, 2339]
- Hamuy, M., Phillips, M. M., Suntzeff, N. B., et al. 1996, *AJ*, 112, 2391
- Hamuy, M., Phillips, M. M., Suntzeff, N. B., et al. 2003, *Nature*, 424, 651
- Hamuy, M., Trager, S. C., Pinto, P. A., et al. 2000, *AJ*, 120, 1479
- Hatano, K., Branch, D., Qiu, Y. L., et al. 2002, *NewA*, 7, 441
- Howell, D. A., Sullivan, M., Nugent, P. E., et al. 2006, *Nature*, 443, 308
- Howerton, S., Drake, A. J., Djorgovski, S. G., et al. 2013, *Central Bureau Electronic Telegrams*, 3507, 1
- Hsiao, E. Y., Phillips, M. M., Marion, G. H., et al. 2019, *PASP*, 131, 014002

- Jeffery, D. J., Leibundgut, B., Kirshner, R. P., et al. 1992, *ApJ*, 397, 304
- Jha, S., Kirshner, R. P., Challis, P., et al. 2006, *AJ*, 131, 527
- Jiang, J.-an., Doi, M., Maeda, K., et al. 2018, *ApJ*, 865, 149
- Kochanek, C. S., Shappee, B. J., Stanek, K. Z., et al. 2017, *PASP*, 129, 104502
- Krisciunas, K., Suntzeff, N. B., Phillips, M. M., et al. 2004, *AJ*, 128, 3034
- Leaman, J., Li, W., Chornock, R., et al. 2011, *MNRAS*, 412, 1419
- Li, W., Filippenko, A. V., Chornock, R., et al. 2003, *PASP*, 115, 453
- Li, W., Filippenko, A. V., Treffers, R. R., et al. 2001b, *ApJ*, 546, 734
- Li, W., Leaman, J., Chornock, R., et al. 2011, *MNRAS*, 412, 1441
- Lira, P., Suntzeff, N. B., Phillips, M. M., et al. 1998, *AJ*, 115, 234
- Mazzali, P. A., Benetti, S., Stehle, M., et al. 2005, *MNRAS*, 357, 200
- Mazzali, P. A., Cappellaro, E., Danziger, I. J., Turatto, M., & Benetti, S. 1998, *ApJL*, 499, L49
- Mazzali, P. A., Danziger, I. J., & Turatto, M. 1995, *A&A*, 297, 509
- Morrell, N., Phillips, M. M., Folatelli, G., et al. 2022, in preparation
- Nicholls, B., Kiyota, S., Brimacombe, J., et al. 2014, *The Astronomer's Telegram*, 6694
- Nugent, P., Phillips, M., Baron, E., Branch, D., & Hauschildt, P. 1995, *ApJL*, 455, L147
- Ochner, P., Tomasella, L., Pastorello, A., et al. 2013, *The Astronomer's Telegram*, 5048
- Pereira, R., Thomas, R. C., Aldering, G., et al. 2013, *A&A*, 554, A27
- Perlmutter, S., Aldering, G., Goldhaber, G., et al. 1999, *ApJ*, 517, 565
- Phillips, M. M. 1993, *ApJL*, 413, L105
- Phillips, M. M. 2012, *PASA*, 29, 434
- Phillips, M. M., Contreras, C., Hsiao, E. Y., et al. 2019, *PASP*, 131, 014001
- Phillips, M. M., Krisciunas, K., Suntzeff, N. B., et al. 2006, *AJ*, 131, 2615
- Phillips, M. M., Li, W., Frieman, J. A., et al. 2007, *PASP*, 119, 360
- Phillips, M. M., Lira, P., Suntzeff, N. B., et al. 1999, *AJ*, 118, 1766
- Phillips, M. M., Wells, L. A., Suntzeff, N. B., et al. 1992, *AJ*, 103, 1632
- Prieto, J. L., Garnavich, P. M., Phillips, M. M., et al. 2007, arXiv e-prints, arXiv:0706.4088
- Riess, A. G., Casertano, S., Yuan, W., et al. 2021, *ApJL*, 908, L6
- Riess, A. G., Filippenko, A. V., Challis, P., et al. 1998, *AJ*, 116, 1009
- Riess, A. G., Macri, L. M., Hoffmann, S. L., et al. 2016, *ApJ*, 826, 56
- Riess, A. G., Press, W. H., & Kirshner, R. P. 1996, *ApJ*, 473, 88
- Ruiz-Lapuente, P., Cappellaro, E., Turatto, M., et al. 1992, *ApJL*, 387, L33
- Saha, A., Sandage, A., Thim, F., et al. 2001, *ApJ*, 551, 973
- Saselli, M., Mazzali, P. A., Pian, E., et al. 2014, *MNRAS*, 445, 711
- Scalzo, R. A., Aldering, G., Antilogus, P., et al. 2010, *ApJ*, 713, 1073
- Scalzo, R. A., Childress, M., Tucker, B., et al. 2014, *MNRAS*, 445, 30
- Schlaflly, E. F., & Finkbeiner, D. P. 2011, *ApJ*, 737, 103
- Schlegel, D. J., Finkbeiner, D. P., & Davis, M. 1998, *ApJ*, 500, 525
- Shappee, B. J., Prieto, J. L., Grupe, D., et al. 2014, *ApJ*, 788, 48
- Shumkov, V., Denisenko, D., Balanutsa, P., et al. 2013, *The Astronomer's Telegram*, 4799
- Silverman, J. M., Foley, R. J., Filippenko, A. V., et al. 2012a, *MNRAS*, 425, 1789
- Silverman, J. M., Kong, J. J., & Filippenko, A. V. 2012b, *MNRAS*, 425, 1819
- Smartt, S. J., Valenti, S., Fraser, M., et al. 2015, *A&A*, 579, A40
- Smith, M., Firth, R., Dimitriadis, G., et al. 2014, *The Astronomer's Telegram*, 6739
- Stahl, B. E., Zheng, W., de Jaeger, T., et al. 2020, *MNRAS*, 492, 4325
- Stritzinger, M., Hamuy, M., Suntzeff, N. B., et al. 2002, *AJ*, 124, 2100
- Suntzeff, N. B., et al. 2022, in preparation

- Takats, K., Romero-Canizales, C., Galbany, L., et al. 2014, The Astronomer's Telegram, 6612
- Taubenberger, S. 2017, Handbook of Supernovae, 317
- Tody, D. 1986, Proc. SPIE, 627, 733. doi:10.1117/12.968154
- Tody, D. 1993, Astronomical Data Analysis Software and Systems II, 52, 173
- Tomasella, L., Benetti, S., Cappellaro, E., et al. 2013, The Astronomer's Telegram, 4796
- Tripp, R. 1998, A&A, 331, 815
- Uddin, S. A., et al. 2022, submitted
- Wyrzykowski, L., Kostrzewa-Rutkowska, Z., Kozłowski, S., et al. 2014, AcA, 64, 197
- Yuan, F., Quimby, R. M., Wheeler, J. C., et al. 2010, ApJ, 715, 1338